Primary Drainage Relative Permeability in Hydrocarbon Reservoirs Interpreted Using Digital Rock Physics

Sven Roth [#], Hu Dong [#], Martin J. Blunt [#,◊], Zubair Kalam*, Ahmed Al Ratrout*[◊], Djelloul Hammadi*
[#] iRock Technologies, Beijing, P.R. China.
[◊] Department of Earth Science and Engineering, Imperial College London, London, UK.
* Abu Dhabi Company for Onshore Oil Operations (ADCO), Abu Dhabi, UAE.

This paper was prepared for presentation at the International Symposium of the Society of Core Analysts held in Vienna, Austria, 27 August – 1 September 2017

ABSTRACT

We apply multi-scale interrogation of complex carbonate reservoir rocks from whole core – plug – micro – nano scale, and then work backwards to upscale and integrate the properties to an acceptable 3D representation. This is achieved through imaging at different resolutions: for each image an equivalent network model is constructed. The smaller-scale networks are upscaled to generate effective properties for input into a plug-scale network representation of the rock.

We study 54 samples from three reservoir zones of a Lower Cretaceous reservoir. Using the Dunham rock classification scheme we see a range of rock types from grainstone to mudstone-dominated. For primary drainage, the higher quality grain-dominated samples show better connectivity and a higher oil relative permeability than the poorer quality rocks. However, for waterflooding the situation is reversed: the better quality rocks tend to be more oil-wet, with a large water relative permeability which leads to early breakthrough and a poor local displacement efficiency. In contrast, the mudstones are mixed-wet and more poorly connected, which impedes the movement of water, leading to a more favourable local recovery.

This study demonstrates how employing the state-of-the-art in multi-scale imaging and modeling, the behavior of complex carbonates can be quantified and interpreted, allowing an assessment of recovery based on pore structure and facies type.

INTRODUCTION

The computation of multiphase properties using Digital Rock Physics and pore-scale modeling, DRP, is extremely valuable as the tests are quick compared with physical laboratory test protocols, and typical costs are about one-half of conventional Special Core Analysis (SCAL) tests using live fluids at full reservoir conditions. Such data are the typical building blocks of dependable field development models of multiphase flow in hydrocarbon reservoirs. Acquisition of accurate representative data minimizes uncertainty in model validations, and opens the possibilities for future sensitivity studies with respect to changes in wettability as well as micro-porosity present in typical Middle Eastern carbonate reservoirs [1, 2].

The goal of this DRP campaign was to complement the SCAL work program for a Lower Cretaceous Reservoir with three reservoir zones (Zone 1, 2, and 3) to provide essential input to the reservoir simulation model.

For every sample, we acquired images at different scales (multi-scale imaging approach), including a full-plug X-ray scan, micro-CT images (tens of micron resolution), micro-CT subsample images (micron resolution) and nano-CT subsample scans (tens of nanometre resolution). An example of such a multi-scale imaging work flow can be found in [3]. Additional QEMSCAN analysis for mineral identification was complemented by high-resolution, large-area electron microscopy mosaics (BSE) to obtain seamless pore-size information.

From the multi-scale rock models, constructed from these images, single and multiphase flow properties were predicted. We predicted electrical properties (resistivity index and the related m and n exponents), elastic properties (elastic constants and acoustic wave speeds), porosity, permeability, capillary pressure and relative permeability, for drainage and waterflooding with detailed scanning curves to investigate relative permeability and capillary pressure hysteresis. Additionally, a series of wettability sensitivity studies have been performed to simulate the effect of low-salinity floods.

For every property, we used an upscaling technique that incorporates the impacts of micro-porosity (characterized at nanometre resolution) with macro-porosity (micron-sized features), together with vugs (mm-sized pores) and fractures. Because wettability is a key control on waterflood capillary pressure and relative permeability it adds a level of complexity when studying the impact of pore structure on relative permeability. The core samples during primary drainage, however, are assumed to be water-wet and so variability in relative permeability is controlled entirely by the pore structure.

In this manuscript, we focus on the effects of rock types and porosity systems on the shape of the water-oil primary drainage relative permeability curves to develop an understanding of how individual rock types and their pore structure shape the primary drainage relative permeability – or vice versa, can primary drainage relative permeability help to refine the current geological- or petrophysical- based rock typing procedure. This could then explain the impact of wettability changes on individual rock types during waterflooding. The combination of pore connectivity at different scales and wettability allows us to identify representative multiphase flow behavior, which is different in primary drainage and waterflooding.

MATERIAL AND METHODS

Formations And Rocks Studied

Twenty-four samples from Reservoir Zone 1, sixteen samples from Reservoir Zone 2, and fourteen samples from Reservoir Zone 3 – a total of 54 samples – were analysed using digital rock physics.

The reservoir zones represent porous units of a Lower Cretaceous formation. Zone 1 has an average thickness of 45ft and Zone 2 has an average thickness of 24ft. Both reservoir zones are composed of limestone, mainly deposited in an open platform, middle ramp to restricted platform subtidal to intertidal environments. Zones 1 and 2 carbonates have been subjected to multiple diagenetic events that have occurred at different post-depositional

times. The present reservoir quality is controlled by four major diagenetic events, including meteoric leaching, cementation, early (meteoric) and late (deep burial) calcite cementation and compaction and stylolitization. Zones 1 and 2 show a high degree of reservoir heterogeneity, which is mainly due to depositional facies and diagenetic overprint. Although most of the lithofacies units show a wide range of porosity and permeability within each lithofacies, they also show large overlapping. Reservoir zone 3 is on average 28 foot thick, and is predominated by bioclastic wackestones to mudstones at the top and base, with intercalated bioclastic pelloidal wackestones to grainstones in the central section. Sequence related reservoir-facies distribution based on geological and petrophysical data properties was used to define flow units and to establish a Reservoir Rock Typing Scheme (RRT). This rock typing scheme is based on the lithofacies identified from core, thin section analysis, and petrophysical results. The reservoir quality of the rock types from Zones 1 and 2 decrease with increasing number, while the permeability of rock types in Zone 2 are generally lower than their counterparts in Zone 1. Within the rock types, moderate to good reservoir quality rock types are mainly developed in the crestal areas (indicated with A) showing preserved primary porosity. Rock types labeled with "B" and "C" are low to moderate reservoir quality rocks with increased cementation and compaction, which occur at the flanks of the reservoirs. The rock typing for Zone 3 is based on lithofacies unit and porosity-permeability range, with smaller numbers being better rock types.

Digital Rocks Work Flow

A generalized work flow for multi-scale imaging and pore-scale modeling is illustrated in Figure 1. Here, the work flow starts with a plug screening using X-ray micro-CT, followed by controlled subsampling and further micro-CT and nano-CT imaging. The acquired images are used to build the multi-scale digital rock models including numerical pore network models, which are then used to calculate and simulate the single phase and multiphase properties. All properties are finally upscaled to the core plug.

Subsampling And Multi-scale Imaging

The multi-scale imaging work flow starts with a full-plug X-ray scan with voxel sizes ranging from 20-40µm. This overview scan provides information about the heterogeneity in the individual core plugs and is used to design a subsampling strategy for the multi-scale imaging. Additionally, this plug CT builds the rock model for later upscaling of all properties. While vugs can be resolved on the plug-overview scan, volumes of macroporosity and microporous matrix can be observed only qualitatively in micro-CT images on the plug level (as areas of different gray shades) - the resolution is not sufficient to resolve the macro- and micropores. For this subsampling and imaging work flow, however, it is mandatory to determine the nature, amount, size, and distribution of all pore types, present in the plug – from vuggy porosity down to microporosity.

The plug X-ray CT was thus complimented with high-resolution, large area backscatter electron microscope images (BSE), acquired with a scanning electron microscope. These BSE mosaics cover large areas (ideally the entire sample surface) down to a resolution that captures even the smallest pores present (nanometer resolution) and provide a continuous

pore-size information of the sample. Although this is a 2D analysis and, as such, derived pore sizes will be slightly offset towards smaller sizes due to stereological effects, all present pore classes can be determined accurately from centimeter to sub-micrometer. This enables us to identify, characterize, and quantify the volumes of sub-resolution pores, which were detected in the plug X-ray CT as volumes of different grey shades.

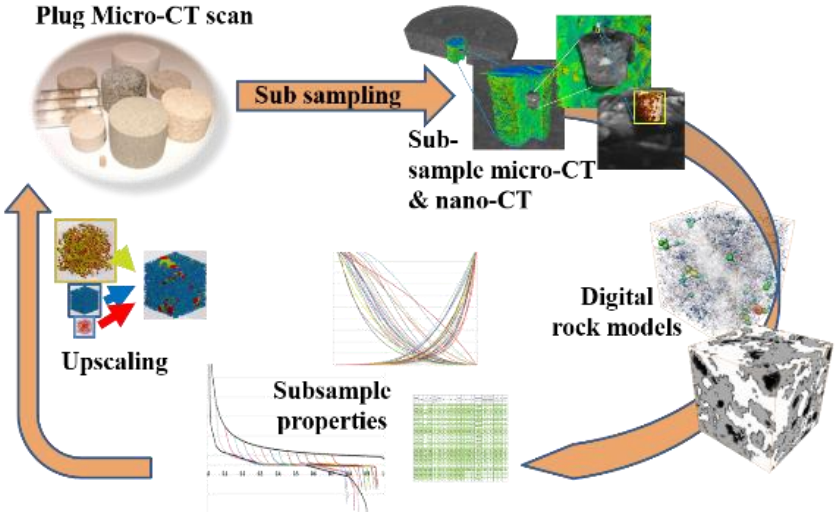

Figure 1. Generalized digital rock work flow, modified from [3].

Additionally, mineralogy was determined on the plug scale using QEMSCAN analysis. QEMSCAN technology provides 2D mineralogy mapping from the same surfaces as used for the BSE images, providing mineral distribution and quantification.

The rock-framework information from the X-ray core-plug screening complimented with the quantitative mineralogy and the detailed BSE-derived pore size information are then utilized to understand the flow characteristics of the core plugs. The most important parameters for successful subsampling are present porosity types, their distribution and interconnection, as well as, the pore sizes in the individual pore classes. This information decides on the location of subsample extraction, the volume of subsamples to be extracted (to be representative for this pore class) and the deployment of imaging instruments, a critical step in the multi-scale 3D rock model construction and subsequent data acquisition. All subsamples were imaged at appropriately high resolution to resolve the pore space. Depending on the facies and pore types, the subsample for micro-CT is typically a cylinder of 2 mm to 16 mm in diameter corresponding to voxel sizes of 1-8 μm. Very fine grained facies, such as micrite and cemented regions, require a much higher resolution than micro-CT equipment can achieve. These facies were imaged using a nano-CT device providing 3D images with a voxel size of 65 nm. Due to the heterogeneity of carbonate rocks, any combination of instrumental 3D image acquisition might be applied – 2 x micro-CT, 1 x micro-CT plus 1 x nano-CT, 2 x nano-CT, etc.

All X-ray micro-CT imaging was performed with a Micro XCT 200, the nano - CT imaging with an Ultra XRM L200, both manufactured by Xradia. The BSE images were acquired

on a Helios NanoLab 650, the mineralogy was investigated with a QEMSCAN 650 F (both from FEI company).

Digital Rock Models And Numerical Pore Networks

Prior to any simulations the 3D X-ray images must be processed and segmented. The processing includes image enhancement (noise reduction) and cropping the 3D volume into a three-dimensional rock model. Noise reduction is performed using an edge preserving smoothing algorithm, which removes noise from the individual rock phases (such as pores, grains) but leaves the phase boundaries untouched. The segmentation into rock phases: pore, microporosity volume, and solid is done using the gray-shade histogram and including the local gradient information. This procedure, noise reduction and filtering, is performed on all multi-scale images. The topology of the pore space is determined using a revised maximal ball algorithm pioneered by [4].

Property Calculations

On these multi-scale rock models, we predicted single and multiphase flow properties, such as electrical properties (resistivity index and the related m and n exponents), porosity, permeability, capillary pressure and relative permeability, for primary drainage. The absolute permeability and formation factor are calculated directly on the grid-based images by solving the Stokes equation and Laplace equations, respectively. The porosity stems directly from segmentation of the individual scale images. The multiphase fluid flow properties are simulated based on the pore scale modeling technology introduced by [5] and adopted and modified by iRock Technologies: capillary-dominated displacement is assumed and so the complexities of ganglion dynamics and viscous effects are ignored.

Upscaling Of Properties

Upscaling of the results is performed using a proprietary three-stage approach. The basis of the method is to construct a multi-scale network model of the rock, see [6] for more details: rather than being an explicit representation of large “pores” connected by “throats” as in traditional pore-network modelling approaches, we instead consider interconnected elements. These elements may indeed be real pores and throats, or could represent an averaged behavior of a region of micro-porosity: this average behavior accurately captures the combined response of the smaller-scale network. In this way, we can construct a network at any scale, representing features spanning many orders of magnitude in scale. Furthermore, we can still retain the semi-analytical computation of conductance and local capillary pressure in each element.

The three stages outlined below and illustrated in Figure 2 deal with the three generic types of porosity encountered in complex carbonate rocks: micro-porosity (Stage 1); combined micro- and macro- porosity (Stage 2); and then combined micro-, macro- and vuggy porosity (Stage 3).

The rock models in Stage 1 capture the smallest pore types present in the rock, which in carbonates is the microporosity. The single-phase properties, absolute permeability and formation factor, etc. is calculated directly on the grid-based representations of the rock. Capillary-dominated two-phase flow through this smallest pore-network system is

simulated to predict two-phase properties such as capillary pressures, relative permeability and resistivity index. The key outputs from this model are capillary pressures and the conductances of oil, water and gas computed as a function of local saturation (which in turn is related to local capillary pressure).

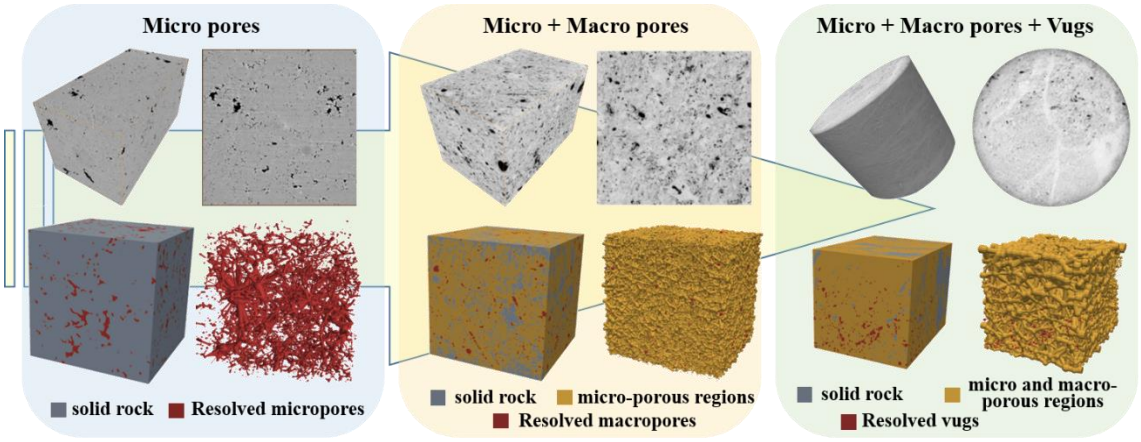

Figure 2. Upscaling work flow illustrating the three-step approach discussed in the text.

The Stage 2 images capture a larger volume of the rock and can resolve macro-pores directly but they cannot directly see the micro-porous voids. However, the presence of micro-porosity can be deduced from intermediate grey-scales in the image. Thus, the image voxels are partitioned into three types: solid voxels, pore voxels and voxels containing micro-scale pores (micro-porosity).

A novel method is used to extract a network of the resolved macro-pore space combined with micro-porosity volumes. We refer to the resolved pore and throats as well as the micro-porosity volumes constituting the combined network simply as "elements". The pore elements detected at this scale are called macro-pores to differentiate them from the micropores generated in Stage 1. The micro-porosity elements from Stage 1 are combined with the macro-porous network; the micro-porosity creates additional connections across the rock resulting in a network of generalized elements whose conductance can be computed as a function of local capillary pressure.

An extended two-phase flow modeling code is used to model the flow through the combined network. The flow through the micro-porosity elements is described using the multiphase Darcy law with the flow properties obtained from the Stage 1. The network model works by gradually increasing the oil pressure in oil-injection cycles and decreasing it in water-injection cycle, which is similar to the displacement sequence in experimental measurements. The water-saturation, the flow and electrical conductivity of the micro-porosity elements are calculated from the capillary pressure curve, the relative permeability and resistivity indices obtained in Stage 1, respectively. The flow equation for the combined network of the macro pores and micro-porosity elements are put together using the mass conservation equation and solved to obtain the single and two-phase flow properties for the Stage 2 micro-CT image.

The same technique is used to upscale the properties of the combined micro- and macro-porosity (Stage 2) to the plug size. By solving the flow equations for the combined network of vugs, micro- and macro- porous elements we obtain the capillary pressure curve, absolute and relative permeabilities, formation factor and resistivity index for the whole sample.

RESULTS AND DISCUSSION

Figure 3 summarises the porosity-permeability of all studied rocks and formations, colour coded after the Dunham classification [7] and labeled according to the rock type scheme described above. The accordance of laboratory derived and upscaled digital porosities and permeabilities for all rocks is illustrated in Figure 4. This comparison is an important step in validating the accuracy of the digital rock models and the data derived from these models [8].

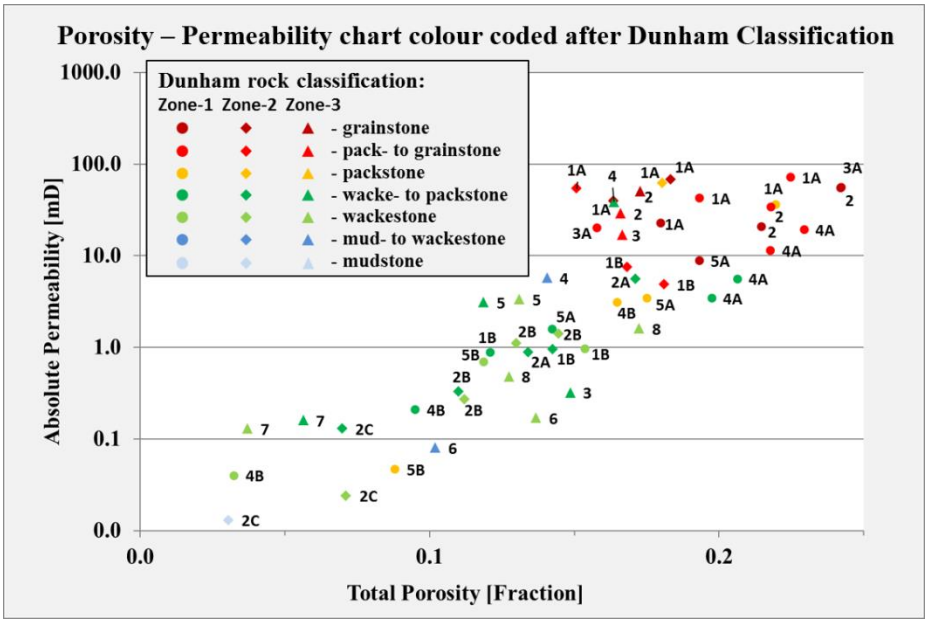

Figure 3. Porosity versus permeability cross plot colour-coded after Dunham Classification and labeled with rock types. Rock type definitions are explained in the text.

The relative permeability curves for all the rocks investigated are shown in Figure 5. As expected the curves show a considerable variability caused by the wide range of rock types and their porosity systems. In order to unravel the behavior of individual rocks the data set was reduced to the cross-over points of the relative permeability curves assuming that this points reflect both, the behavior of the water- and oil relative permeability curves.
Figure 6 shows the extracted cross-over points marked after reservoir zones (different symbols) and color-coded. Two methods were used to discriminate between the rocks: (1) a characterization according to tri-modal versus bi-modal pore systems (left graph) and (2) according to the classical Dunham classification (right graph). The classification into tri- versus bi- modal pore system (1) was further subdivided depending on which pore class is

dominating the overall porosity system – macroporosity or microporosity or vugs. Then each of the encoded assemblages were enclosed into lower and upper bounding curves to find the fields where the categorized crossover-points plot.

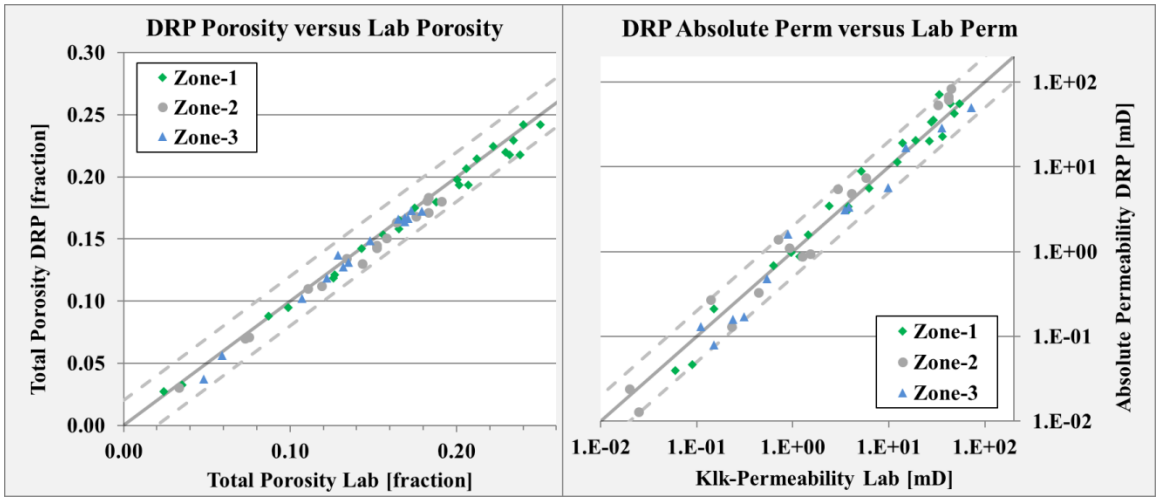

Figure 4. Comparison of laboratory derived total porosities (left) and permeabilities (right) versus digital rock data. The gray solid lines are the 1:1 relations, the broken lines indicate the envelopes for ± 2 units deviation in porosity (left graph) and a factor of two for permeability (right graph).

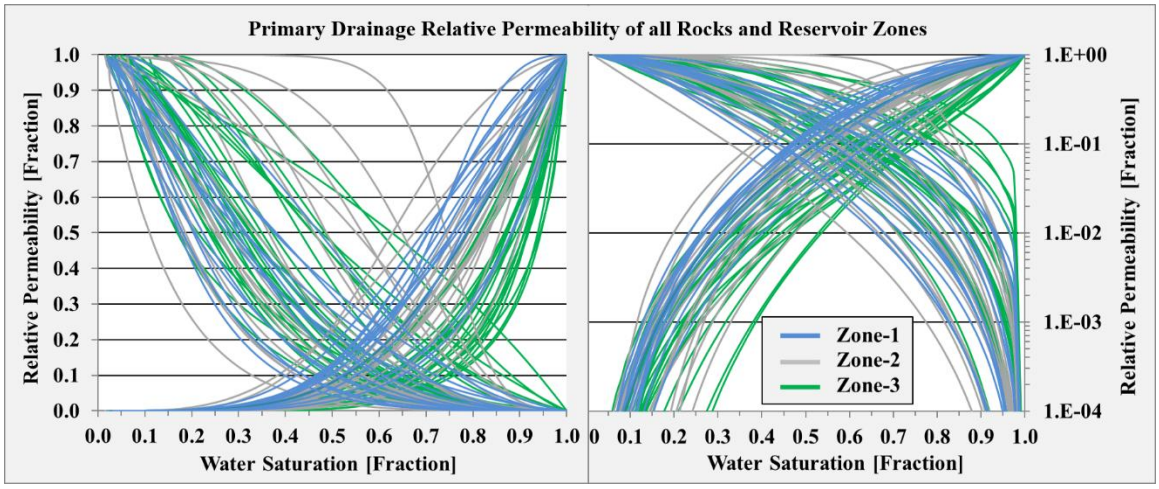

Figure 5. Primary drainage relative permeability of Reservoir Zones 1, 2, and 3.

While classification into tri- and bi- modal pore systems (1) is relatively straightforward, the Dunham classification (2) is more like a continuous transition. Here the boundary was drawn between the grain-dominated and mud-dominated rocks. The latter comprise mudstones, wackestones and wacke- to packstones (blue bounding curves and field), while grainstone, pack- to grainstone and packstone belong to the grain-dominated rocks (red bounding lines and red field). Both categorizations result in very similar fields of cross-over points. Although it was expected that the much more detailed classification in pore systems (1) would result in more distinct cross-over accumulation fields, Figure 6 exhibits

that further subdivision into macroporosity- or microporosity- dominated bi- and tri- modal pore system does not yield advantages over the 'coarser' Dunham classification. The likely explanation for this is that we are only considering volumes of pore classes, neglecting the important effect of how these volumes are distributed and interconnected. We therefore follow the easier Dunham classification for the rest of this manuscript.

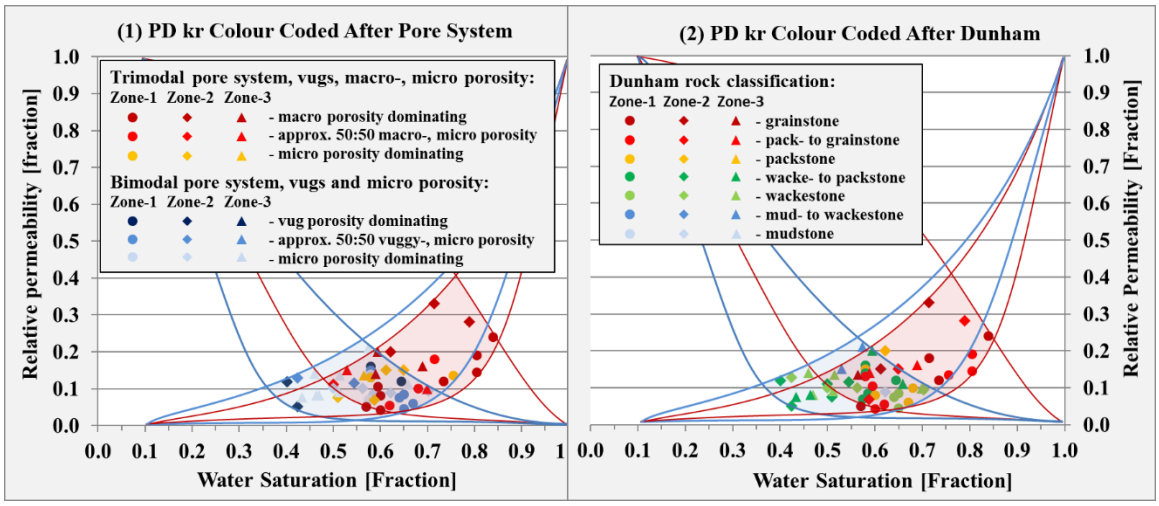

Figure 6. Primary drainage relative permeability cross-over points of all three reservoir zones colour coded after pore system (left) and Dunham classification (right).

In the next step we populated the Dunham-colour coded primary drainage cross-over points with absolute permeability, formation factor data, as well as rock types and wettability indication (Figure 7). The permeability and the formation factor show a clear inverse overall trend from higher saturation/higher relative permeability towards lower saturation/lower relative permeability cross-over points. The mud-dominated rock types (blue to green colours and blue field) plot in a narrower range of water saturations between 0.4 - 0.7, and relative permeability between 0.05-0.2. The grain dominated rocks (orange to red colours and red field) show a larger variability between 0.57-0.84 water saturation and 0.04-0.33 relative permeability. This is insofar intuitive as the mud-dominated rocks have only one governing pore system – the microporosity, while the grain dominated facies usually have two generations of conducting pore systems: macroporosity and microporosity. The behavior of their relative permeability curves and thus the location of the cross-over points are governed by the contribution of each of the pore systems to the overall rock, which is dependent on their relative volume, their hydraulic properties and their interconnection.

Figure 7 (lower left), also illustrates the link between the rock types and the location of cross-over points. The individual rock types plot well within the blue, mud-dominated and the red, grain dominated fields, which were based on the bounding curves of pore classes and Dunham classification.

The implication for wettability is shown on the lower right of Figure 7. At a distinct level in the reservoir (at any given capillary pressure) the grain dominated facies tend to be more mixed to oil wet, while the mud-dominated rocks show a more mixed to water wet behavior.

The wettability indication plotted in Figure 7 is based on the understanding of the reservoirs and rock types. Insofar the shape of the primary drainage curves or their cross-over points analysed through pore-network modeling could be used to indicate wettability for subsequent modeling of waterflooding.

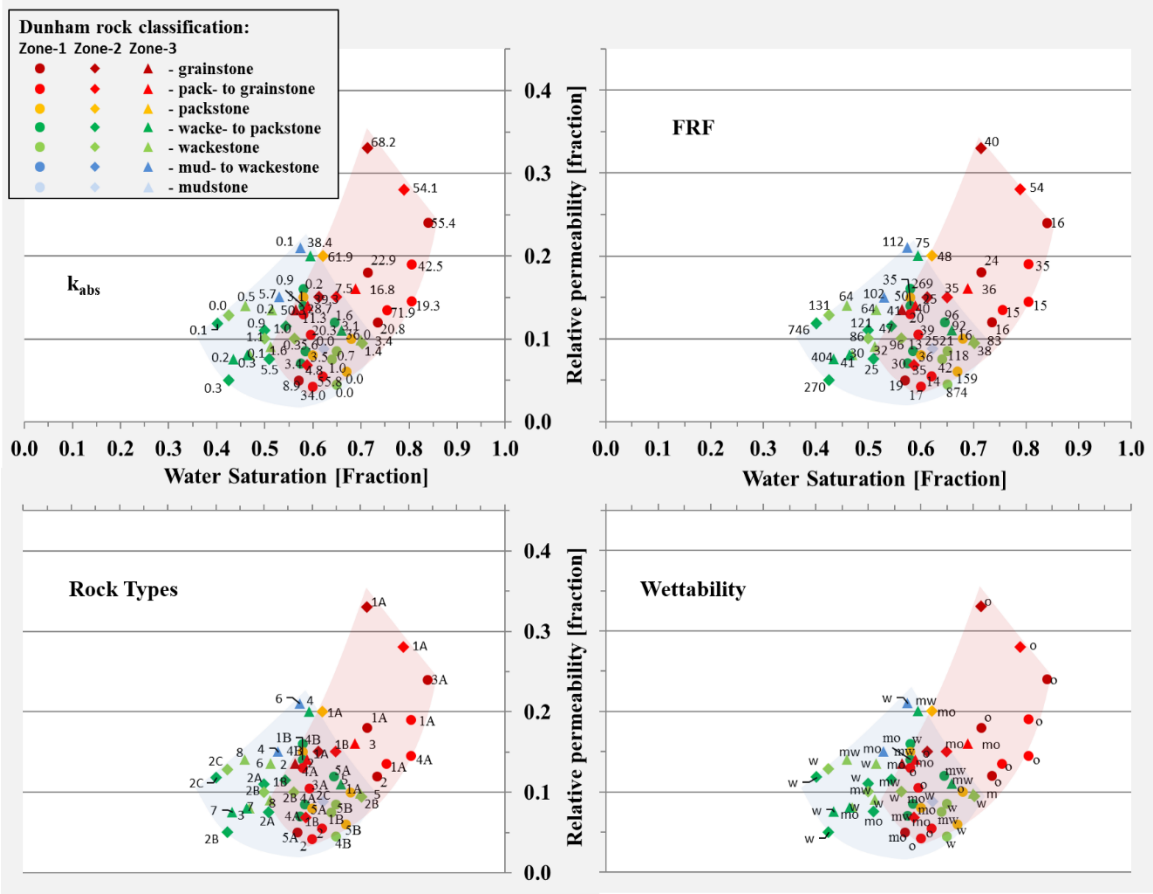

Figure 7. Primary drainage relative permeability cross-over points colour coded after Dunham classification and labeled with absolute permeability (upper left), formation factor (upper right), rock types (lower left) and wettability (lower right; o: oil wet, mo: mixed to oil wet, mw: mixed to water wet, w: water wet). The reservoir quality of the rock types generally decreases with increasing number. For Zones 1 and 2, "A" indicates moderate to good, while "B" and "C" are low to moderate reservoir conditions.

Figure 8 illustrates the results of waterflood modeling with the given wettability indications. The different behavior of the waterflood relative permeability curves between mixed to water-wet (blue) and mixed to oil-wet (red) rocks.

The results help to indicate the likely waterflood performance of the samples. The more grain-dominated facies are likely to have a lower initial water saturation in the reservoir and tend to be oil-wet during waterflooding. Now the good connectivity of the larger pore spaces allows the rapid movement of water, leading to high water relative permeabilities and a low cross-over saturation, which is associated with poor local displacement efficiency, see Figure 8 and page 329 in [9]. Instead, the mud-dominated samples are mixed to water-wet and have a less well-connected path of larger pores. This leads to a lower

water relative permeability, a higher cross-over saturation and more favourable recovery. Note that this is the opposite trend than seen for primary drainage and indicates the significance of both pore structure and wettability in the behavior.

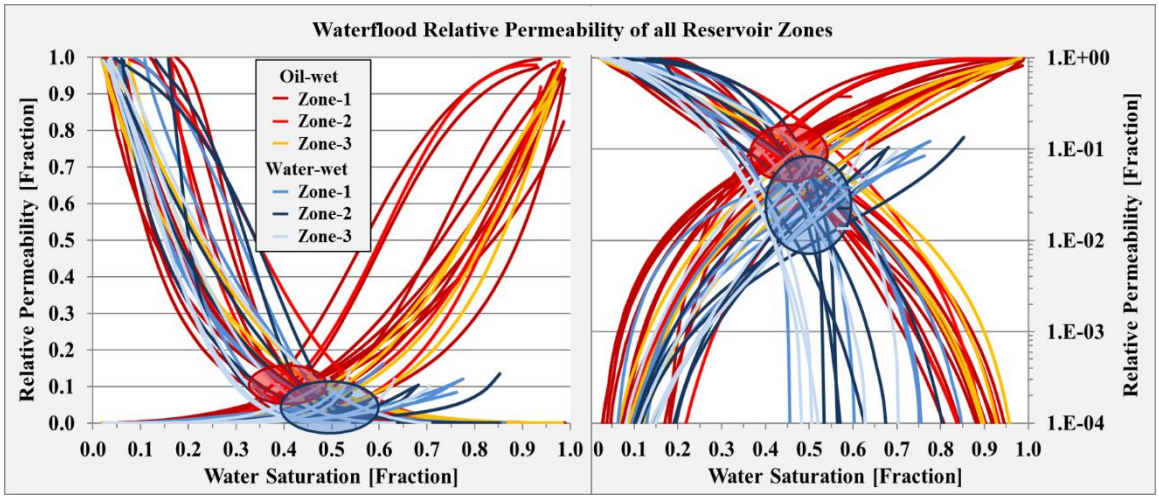

Figure 8. Waterflood relative permeability of Reservoir Zones 1, 2, and 3. Red and blue circles indicate the fields of cross-over points for the oil-wet samples and the water-wet samples, respectively.

It has been demonstrated in this study that individual rock types and their petrophysical properties have a distinct impact on the corresponding relative permeability curves, which then could be used for more dynamic rock classification/rock typing.
In this study, we have discriminated only between mud-dominated and grain-dominated facies based on the presence of different pore classes (digital; Figure 6, left) and based on the geological Dunham classification (Figure 6, right). This was then backed-up with absolute permeability measured in the laboratory, formation factor (digital) and the rock typing (petrophysical) and wettability indication. The data set presented here is promising - however, especially the grain-dominated facies show a too large variability (too wide a cross-over field) to be used for improved rock typing. A possible solution would be to study more in detail the contribution of individual pore classes within bi-, and tri- modal pore systems – not only volumetrically as done in this study but based on volume, distribution and connectivity of individual pore classes, incorporating their hydraulic properties.

CONCLUSIONS

We have demonstrated how the rapid and comprehensive prediction of multiphase flow properties using Digital Rock Physics, employing a multi-scale imaging and modeling work flow, can be used to interpret and quantify trends in behavior and assign rock types.
In this study we show that the more grain-dominated facies give – for primary drainage relative permeability – a cross-over at high water saturation, indicating high-conductivity pathways of the larger pore spaces. These rocks tend to be more oil-wet for subsequent waterflooding which reverses the behavior: the cross-over is now pushed to low water saturation, indicating poor recovery, as the larger pores are filled rapidly by water as the

non-wetting phase. The more mud-dominated samples show the opposite behavior, tend to be more mixed to water wet, and provide more favourable waterflood recoveries.
This work offers a promising application of modeling technology and could be applied to a wider range of rocks using a more detailed classification of the pore structure and its connectivity.

ACKNOWLEDGEMENTS

We would like to thank ADCO and ADNOC Management for supporting our digital rock studies on their reservoir rocks and for permission to publish this work. We are also grateful to Maher Kenawy and Moustafa Haggag, from ADCO for providing the geological descriptions and the provision of the reservoir cores.

REFERENCES

1. Kalam, M.Z., "Digital Rock Physics for Fast and Accurate Special Core Analysis in Carbonates", In: *New Technologies in the Oil and Gas Industry*, J.S. Gomes (eds), (2012), DOI:10.5772/52949.
2. Al-Ratrout, A.A., M.Z. Kalam, J.S. Gomes, M.S. Jouini, S. Roth, (2014). "Narrowing the Loop for Microporosity Quantification in Carbonate Reservoirs Using Digital Rock Physics and Other Conventional Techniques – Part II", *International Petroleum Technology Conference, Doha, Qatar*, (2014), IPTC 17702.
3. Roth, S., Y. Hong, H. Bale, T. Zhao, S. Bhattiprolu, M. Andrew, C. Weichao, J. Gelb and B. Hornberger, "Fully Controlled Sampling Workflow for Multi-Scale X-Ray Imaging of Complex Reservoir Rock Samples to be Used for Digital Rock Physics", *Search and Discovery*, (2016), Article #41840.
4. Dong, H. and M.J. Blunt. "Pore-network extraction from micro-computerized-tomography images", *Physical Review E*, (2009), **80**, 3, 036307.
5. Valvatne, P.H. and M.J. Blunt, "Predictive pore-scale modeling of two-phase flow in mixed wet media," *Water Resources Research*, (2004), **40**, 7, W07406.
6. Roth, S. "Porous Media Analysis System and Method." *International Patent Filing No.:PCT/CN2015/089409, filed September 2015*.
7. Dunham, R.J., "Classification of carbonate rocks according to depositional texture", In *Classification of carbonate rocks*, W.E. Ham (eds), American Association of Petroleum Geologists, **Memoir 1**, (1962), pp. 108–121.
8. Kalam, M. Z., T. Al Dayyani, A. Clark, S. Roth, C. Nardi, O. Lopez, P.-E. Øren, "Case study in validating capillary pressure, relative permeability and resistivity index of carbonates from X-Ray micro-tomography images", *SCA International Symposium, Halifax, Canada*, (2010), paper SCA2010-02.
9. Blunt, M.J., *Multiphase Flow in Permeable Media – A pore-scale perspective*, Cambridge University Press, Cambridge, (2017), DOI: 10.1017/9781316145098.